Precise simulation of criticality in asymmetric fluids

G. Orkoulas, Michael E. Fisher, and A. Z. Panagiotopoulos
Institute for Physical Science and Technology, University of Maryland, College Park, Maryland 20742-2431
(Received 10 November 2000; published 26 April 2001)

Extensive grand canonical Monte Carlo simulations have been performed for the hard-core square-well fluid with interaction range $b=1.5\sigma$. The critical exponent for the correlation length has been estimated in an unbiased fashion as $\nu=0.63\pm0.03$ via finite-size extrapolations of the extrema of properties measured along specially constructed, asymptotically critical loci that represent pseudosymmetry axes. The subsequent location of the critical point achieves a precision of five parts in 10^4 for T_c and about 0.3% for the critical density ρ_c. The effective exponents $\gamma_{\rm eff}^{+}$ and $\beta_{\rm eff}$ indicate Ising-type critical-point values to within 2% and 5.6%, respectively, convincingly distinguishing the universality class from the ''nearby'' XY and $n=0$ (self-avoiding walk) classes. Simulations of the heat capacity $C_V(T,\rho)$ and d^2p_σ/dT^2, where p_σ is the vapor pressure below T_c, suggest a negative but small Yang-Yang anomaly, i.e., a specific-heat-like divergence in the corresponding chemical potential derivative $(d^2\mu_\sigma/dT^2)$ that requires a revision of the standard asymptotic scaling description of asymmetric fluids.

DOI: 10.1103/PhysRevE.63.051507 PACS number(s): 02.70.Rr, 05.70.Jk, 64.60.Fr, 64.70.Fx

I. INTRODUCTION

Liquid-vapor and liquid-liquid phase separation and the related critical behavior in real fluids is *not* describable by any direct ''broken symmetry'' of the sort that characterizes so many phase transitions in magnetic and other condensed matter systems. This fact poses significant problems both experimentally and theoretically. At the most basic level, locating the critical point of a fluid entails the determination of *two* separate parameters, say the critical temperature T_c and the critical density ρ_c, whereas in a ferromagnet or a superfluid only T_c must be found since the ''axis of symmetry,'' on which the critical point resides, specified, e.g., by zero magnetic field or vanishing off-diagonal field, is both readily identified theoretically and easily realized experimentally. Nevertheless, experimental observations of real fluids do reveal a high degree of *asymptotic symmetry*. Most notably, if $\rho_{\rm liq}(T)$ and $\rho_{\rm vap}(T)$ denote the two sides of the coexistence curve beneath T_c, the ratio

$$\mathcal{R}_\rho \equiv [\rho_{\rm liq}(T)-\rho_c]/[\rho_c-\rho_{\rm vap}(T)] \tag{1.1}$$

approaches unity rapidly as $T\to T_c^-$. More explicitly, the width of the coexistence curve, $\rho_{\rm liq}(T)-\rho_{\rm vap}(T)$, vanishes as $|t|^\beta$ with $\beta\simeq 0.32_6$, where

$$t=(T-T_c)/T_c, \tag{1.2}$$

while the diameter

$$\overline{\rho}(T)\equiv \tfrac{1}{2}[\rho_{\rm liq}(T)+\rho_{\rm vap}(T)] \tag{1.3}$$

approaches ρ_c as $\rho_\psi|t|^\psi$ where, in practice, ψ can hardly be distinguished from unity and ρ_ψ/ρ_c is numerically small. Theoretically, the consensus for many years was that $\psi=1-\alpha\simeq 0.89_1$, but recent work [1] suggests, rather, that $\psi=2\beta\simeq 0.65$; however, competing additive terms in $\overline{\rho}(T)$ varying as $|t|^{1-\alpha}$ and as t preclude convincing experimental tests [1].

Indeed, even with a scaling theory that recognizes asymptotic symmetry, the origin of the $|t|^{2\beta}$ correction lies in a deep lack of full symmetry in terms of the ''obvious'' physical variables [1]: this manifests itself most directly in a *divergence* as $T\to T_c^-$ of the second derivative $(d^2\mu_\sigma/dT^2)$ of $\mu_\sigma(T)$, the chemical potential at which the vapor and liquid phases coexist. As Yang and Yang [2] pointed out in 1964, such a divergence is forbidden by the (artificial) symmetry of the standard lattice gas (which is isomorphic to an Ising-type ferromagnet). The divergence of $(d^2\mu_\sigma/dT^2)$, which we term a Yang-Yang anomaly [1], is also absent in various related model fluids that possess a ''hidden symmetry'' [3–5]. Nevertheless, as stressed by Yang and Yang [2] and uncovered in recent analyses of the specific heats of propane and carbon dioxide [1,6], real fluids need not and, indeed, do not respect even the expected hidden symmetry. Nor are there good reasons to suppose that more realistic continuum models, such as the Lennard-Jones fluid or the hard-core square-well (HCSW) gas [7], which we investigate here, will exhibit an asymptotic hidden symmetry.

This situation is particularly pressing in the case of the most basic model of an electrolyte or ionic fluid, namely, the restricted primitive model (RPM) [8–13] where the coexistence curve is known (by simulations [14–17]) to be *extremely* asymmetric. At the same time, the nature of fluid criticality in the RPM—whether of Ising type or classical (i.e., mean-field or van der Waals), crossover from one to the other, or something new—is still open to serious question [8–13]. Indeed, a principal motivation for the present study was to discover and test effective simulation techniques for more revealing and definitive investigations of the RPM electrolyte [18].

In previous work [19] we studied three-dimensional *symmetric* lattice gases (or Ising ferromagnets) with many neighbor (i.e., intermediate range) interactions using *limited* computational resources. The aim, successfully achieved, was to show that even without large-scale computing capabilities, the systematic employment of appropriate finite-size scaling techniques could enable one to convincingly elucidate the

universality class, and detect *crossover phenomena*. Thus, in a simple cubic lattice gas with up to 26 equivalent-neighbor, i.e., equally strong, couplings [19], the fundamental correlation length exponent ν could be determined as $\nu = 0.63 \pm 0.02$; that is close to the best estimates for Ising systems (say $\nu_{\rm Is} = 0.6303 \pm 0.0010$ [20]) and is certainly adequate to distinguish the behavior from the two most well-known ''nearby'' potential candidates, namely, self-avoiding walks (or $n=0$ systems) and XY spin models ($n=2$) with $\nu_{\rm saw} \simeq 0.58_8$ and $\nu_{\rm XY} \simeq 0.67_6$, respectively [20]. The classical (mean-field or van der Waals) value $\nu_{\rm mf} = \frac{1}{2}$ was unambiguously excluded.

However, crossover behavior from Ising-type character to classical forms, depending on the range of the interaction R_0, could also be clearly identified by studying the temperature dependence of the effective exponents $\beta_{\rm eff}(T)$ for the coexistence curve, and $\gamma^{+}_{\rm eff}(T)$ and $\gamma^{-}_{\rm eff}(T)$ for the susceptibility and/or compressibility divergence [19, 21–23]. The finite-size rounded effective exponent data could be readily extrapolated to reveal Ising-type values at thermodynamic criticality. Furthermore, the estimated critical temperatures agreed encouragingly well with values obtained in large-scale computations [21–23].

Here we bring the techniques developed in [19] to bear on the HCSW fluid with an interaction-to-hard-core diameter ratio $\lambda = b/\sigma = 1.5$ [7]. It is immediately evident, however, that the first and critical problem is to devise methods to locate the critical density and to determine appropriate loci in the phase plane upon which to study the finite-size temperature dependence [24].

Now on the *assumption* that the asymptotic critical behavior is of Ising character, Bruce and Wilding (BW) [25, 26] have developed a general method for estimating T_c and ρ_c using the histogram of density (and energy) fluctuations calculated by simulation in a grand canonical ensemble of finite dimensions, $L \times L \times L$ (in $d=3$ dimensions), with periodic boundary conditions. We will, indeed, employ such simulations (see, e.g., [17]). However, in the first place, we are anxious, with applications to the RPM in mind, *not* to presuppose that criticality in the HCSW fluid is of Ising type; second, even if it is (as we will actually establish with encouraging precision) the BW technique *further assumes* the absence of any Yang-Yang anomaly. More specifically, in their scaling formulation [25, 26] Bruce and Wilding do *not* allow for any mixing of the pressure p into the asymptotic linear scaling fields as is necessary to understand the appearance of the anomaly [1]. Since we would like to assess the possible magnitude of a Yang-Yang anomaly in the HCSW fluid, presupposing its absence is obviously inappropriate. Finally, we will, in fact, demonstrate that the biases introduced, inadvertently or otherwise, by the BW approach lead to a significant overestimate of the critical density ρ_c. (And one may well suspect the same is true in applications of the method to the RPM [15,17, 27].)

Following [19], therefore, but recognizing the intrinsic asymmetry of criticality in the HCSW fluid, we have devised a range of unbiased methods for estimating the critical density. These mainly rest on the calculation for finite $L \times L \times L$ systems of various loci in the (T,ρ) plane which, in the thermodynamic limit, $L \to \infty$, must spring from the true critical point (T_c, ρ_c) [27]. By introducing an adjustable parameter we find, indeed, an optimal locus that can be regarded as approximating an axis of pseudosymmetry of the sort that arises in exactly soluble models with an explicit or hidden symmetry [3–5]. The finite-size scaling techniques used in [19] can now be employed effectively on the various asymptotically critical loci—first to obtain an unbiased estimate of ν and, thence, estimates of T_c and ρ_c: see Sec. III.

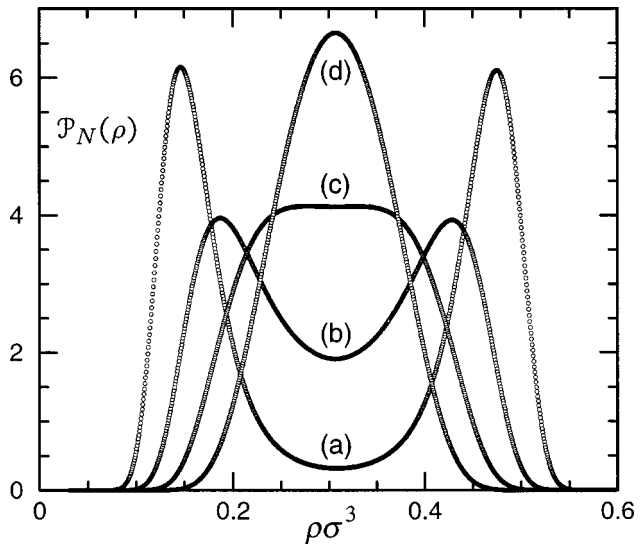

FIG. 1. Equal-height grand canonical density distributions for a system size of $L = 12\sigma$: (a) $T^* = 1.18$; (b) $T^* = 1.20$; (c) $T^* = 1.238$; (d) $T^* = 1.26$. The value of the chemical potential that corresponds to equal heights was found by histogram reweighting. Since $T > T_c^0(L)$ for case (d), the chemical potential was chosen to yield an average density equal to the critical value.

We also mention here, because of its potential interest to the study of pseudo- or ''near'' phase transitions in *finite* clusters of particles (such as gas-phase ''droplets,'' atomic nuclei, etc., see, e.g., [28–30]) a supplementary method of obtaining sequences of ''canonical'' estimates, say $T_c^0(L)$ and $\rho_c^0(L)$, which can also be extrapolated to aid in estimating the true T_c and ρ_c. Specifically, as described in Sec. II B, one may exploit a canonical formulation in which the two peaks of the density histogram for $T < T_c$ approach, merge at a ''finite-size critical point,'' $T_c^0(L)$ and $\rho_c^0(L)$, and reduce to a *single*, effectively Gaussian peak: see Fig. 1. Of course, the behavior in the vicinity of (T_c^0, ρ_c^0) is completely classical (although when $L \to \infty$, the effective, close-to-parabolic coexistence curves, for example, approach the limiting Ising-type form: see Fig. 7).

Armed with precise and, we believe, rather reliable estimates of T_c and ρ_c one can go on to examine the effective exponents $\gamma^{+}_{\rm eff}(T)$ and $\beta_{\rm eff}(T)$ to check consistency with the Ising universality class as indicated by the estimated value of the correlation exponent, namely, $\nu = 0.63 \pm 0.03$. This is less precise than could be obtained in the symmetric lattice gases [19]; but it is still adequate to discriminate against the self-avoiding-walk ($n=0$) or XY ($n=2$) values mentioned above.

Finally, in Sec. IV we discuss, following the analysis in [1], the constant volume specific heat $C_V(T,\rho)$ and, using appropriate expressions in terms of third-order moments of the joint density and energy histograms, the derivative $(d^2\mu_\sigma/dT^2)$ involved in defining the Yang-Yang anomaly as discussed above. Unfortunately, the data are not as precise—the third-order histogram moments being, inevitably, more noisy than the lower-order moments—nor as extensive in terms of accessible size range—limited to $L \lesssim 15\sigma$—as we would wish. Nevertheless, the presence of a negative, albeit rather weak Yang-Yang anomaly (similar to that found in CO_2 [6]) does appear likely to be present in the hard-core square-well fluid with relative interaction range $\lambda = 1.5$. Some brief concluding remarks are presented in Sec. V.

II. MODEL AND METHODOLOGIES

A. Moments and fluctuations in the grand ensemble

The hard-core square-well (HCSW) fluid has been studied extensively [7] since it is arguably the simplest continuum model that exhibits realistic gas-liquid phase separation and criticality. The pair interaction potential between two particles (spheres of diameter σ) is infinite for distances $r \leqslant \sigma$, attractive of strength ε for $\sigma < r \leqslant \lambda\sigma$, and zero thereafter. In modeling systems characterized by short-range forces, the parameter λ is typically taken to be 1.5. Upon defining a reduced pressure and inverse temperature or coupling strength

$$\overline{p} = p/k_B T, \quad \theta = \varepsilon/k_B T = 1/T^*, \tag{2.1}$$

and on absorbing the de Broglie thermal wavelength $\Lambda(T)$ into the definition of the chemical potential μ through

$$\tilde{\mu} = \mu/k_B T - 3\ln(\Lambda/\sigma), \tag{2.2}$$

the grand partition function at fixed (reduced) chemical potential $\tilde{\mu}$, volume $V = L^3$, and coupling θ, can be written as

$$\Xi(\tilde{\mu},\theta;L) = \exp(\overline{p}V) = \mathrm{Tr}[\exp(\tilde{\mu}N - \theta U)], \tag{2.3}$$

where the trace represents summation over all particle numbers N and integration over all continuum states of configurational energy U.

The first derivatives of the grand potential $\overline{p}$ give the mean density ρ and energy density u via

$$\frac{\partial\overline{p}}{\partial\tilde{\mu}} = \frac{\langle N\rangle}{V} = \rho, \tag{2.4}$$

$$\frac{\partial\overline{p}}{\partial\theta} = -\frac{\langle U\rangle}{V} = -u, \tag{2.5}$$

where the notation $\langle\cdot\rangle$ will always imply an average over the finite-size grand canonical distribution of states.

The second derivatives determine the usual response functions (or susceptibilities, compressibilities, heat capacities, etc.). Specifically we have

$$\frac{\partial^2\overline{p}}{\partial\tilde{\mu}^2} = \frac{\partial\rho}{\partial\tilde{\mu}} = \frac{1}{V}\langle(\delta N)^2\rangle \equiv \chi_{NN}, \tag{2.6}$$

$$\frac{\partial^2\overline{p}}{\partial\theta^2} = -\frac{\partial u}{\partial\theta} = \frac{1}{V}\langle(\delta U)^2\rangle \equiv \chi_{UU}, \tag{2.7}$$

$$\frac{\partial^2\overline{p}}{\partial\tilde{\mu}\partial\theta} = \frac{\partial\rho}{\partial\theta} = -\frac{\partial u}{\partial\tilde{\mu}} = -\frac{1}{V}\langle\delta N\,\delta U\rangle \equiv -\chi_{NU}, \tag{2.8}$$

where $\delta X = X - \langle X\rangle$. The familiar isothermal compressibility, $K_T = \rho^{-1}(\partial\rho/\partial p)_T$, is related to χ_{NN} via

$$\chi_{NN} = k_B T \rho^2 K_T. \tag{2.9}$$

Higher-order susceptibilities will often be of interest in the critical region. To that end it is felicitous to define a generalized susceptibility as

$$\chi_{N^k U^m} = \langle(\delta N)^k(\delta U)^m\rangle/V, \tag{2.10}$$

with the general Maxwell relations

$$\chi_{N^k U^m} = \frac{\partial}{\partial\tilde{\mu}}(\chi_{N^{k-1}U^m}) = -\frac{\partial}{\partial\theta}(\chi_{N^k U^{m-1}}) = (-1)^m(\partial^{m+k}\overline{p}/\partial\tilde{\mu}^k\partial\theta^m). \tag{2.11}$$

For studies in phase transitions and critical phenomena, temperature derivatives at fixed chemical potential are frequently not the most informative quantities; one would rather prefer—in accordance with typical experimental observations—to follow a path of constant density ρ. For a function $g = g(\tilde{\mu},\theta)$ one evidently has

$$\left(\frac{\partial g}{\partial\theta}\right)_\rho = \left(\frac{\partial g}{\partial\tilde{\mu}}\right)_\theta\left(\frac{\partial\tilde{\mu}}{\partial\theta}\right)_\rho + \left(\frac{\partial g}{\partial\theta}\right)_{\tilde{\mu}}. \tag{2.12}$$

The derivative $(\partial\tilde{\mu}/\partial\theta)_\rho$ may be found by setting $g = \rho$ to obtain $(\partial\tilde{\mu}/\partial\theta)_\rho = \chi_{NU}/\chi_{NN}$. For reference below we record the general result

$$\left(\frac{\partial g}{\partial\theta}\right)_\rho = \frac{\chi_{NU}}{\chi_{NN}}\left(\frac{\partial g}{\partial\tilde{\mu}}\right)_\theta + \left(\frac{\partial g}{\partial\theta}\right)_{\tilde{\mu}}. \tag{2.13}$$

For example, on setting $g = -\langle U\rangle/V$, and using Eqs. (2.6)–(2.11), one obtains the configurational part of the constant-volume heat-capacity density, namely,

$$\check{C}_V = \chi_{UU} - \chi_{NU}^2/\chi_{NN}. \tag{2.14}$$

The overall heat capacity at constant volume $\mathcal{C}_V^{\mathrm{tot}}$ is then given by

$$\mathcal{C}_V^{\mathrm{tot}}/k_B V = \tfrac{3}{2}\rho + \check{C}_V/k_B T^{*2}. \tag{2.15}$$

B. Data analysis and phase coexistence

We analyze our raw simulation data using histogram reweighting techniques [31] that are now routinely applied to extracting the maximum amount of information from a molecular simulation. In the framework of the grand canonical

ensemble, one performs a simulation at a thermodynamic state characterized by a given value of the chemical potential, say, $\tilde{\mu}_0$ and the inverse temperature (coupling), $\theta_0 = \varepsilon/k_B T_0$, and measures the joint histogram $\mathcal{P}_0(N,U)$ of the fluctuating energy U and number of particles N. The histogram $\mathcal{P}(N,U;\tilde{\mu},\theta)$ of a different state $(\tilde{\mu},\theta)$, not too far away from $(\tilde{\mu}_0,\theta_0)$, may be obtained from $\mathcal{P}_0(N,U)$ through the simple reweighting formula

$$\frac{\mathcal{P}(N,U;\tilde{\mu},\theta)}{\mathcal{P}_0(N,U)} \propto \exp[(\tilde{\mu}-\tilde{\mu}_0)N-(\theta-\theta_0)U] \quad (2.16)$$

without any need to perform an independent simulation at $(\tilde{\mu},\theta)$. The properties of interest, such as those introduced in Eqs. (2.4)–(2.11), can then be obtained by simple averaging, via

$$\langle X\rangle_{\tilde{\mu},\theta} = \frac{\sum_{N,U} X(N,U)\mathcal{P}(N,U;\tilde{\mu},\theta)}{\sum_{N,U} \mathcal{P}(N,U;\tilde{\mu},\theta)}. \quad (2.17)$$

Near and at a first-order phase transition, the grand canonical density distribution attains a characteristic broad, double-peaked structure; the local minimum that separates the two peaks is generally attributed to the formation of interfaces [32]. For $T \ll T_c$, when the peaks are well separated, ''the equal-weight criterion'' [33] may be used to determine the chemical potential, say, $\tilde{\mu}_\sigma(\theta)$ of the phase transition. Specifically, for a given temperature, one calculates the area under each peak—which, in view of Eq. (2.3), is essentially proportional to the pressure—and locates—in the framework of the histogram reweighting scheme—the value of the chemical potential for which the two areas are equal: this identifies the phase boundary $\tilde{\mu}_\sigma(\theta)$.

It should be noted, however, that an alternative definition of the phase boundary, fixed by an ''equal height criterion'' [34], is also reasonable. As the name indicates, one identifies, say, $\tilde{\mu}^0_\sigma(\theta)$, as the particular value of the chemical potential for which the underlying grand canonical density distribution has two peaks of equal height. In view of the connection between the canonical and the grand canonical ensemble it can be shown readily that the equal-height construction merely corresponds to canonical ensemble coexistence [34]. To better appreciate this, consider the statistical-mechanical form of the grand canonical distribution of densities

$$\mathcal{P}_N(\rho) \equiv \sum_U \mathcal{P}(N,U;\tilde{\mu},\theta) \propto \exp[-\overline{f}_{\rm can}(\rho,\theta)V+\tilde{\mu}N], \quad (2.18)$$

where now $\rho = N/V$ and $\overline{f}_{\rm can}(\rho,\theta)$ is the (canonical) free-energy density. Note that $\overline{f}_{\rm can}$ can be obtained by performing a grand canonical simulation at $\tilde{\mu}$ and measuring the histogram $\mathcal{P}_N(\rho)$. The canonical chemical potential and pressure are thereby defined by

$$\tilde{\mu}_{\rm can} = (\partial \overline{f}/\partial\rho)_\theta \quad \text{and} \quad \overline{p}_{\rm can} = -\overline{f}_{\rm can} + \tilde{\mu}_{\rm can}\rho. \quad (2.19)$$

For a finite system analyticity is anticipated and $\tilde{\mu}_{\rm can}(\rho)$ will exhibit van der Waals–type loops. Let $\tilde{\mu}_0$ be the chemical potential that satisfies a Maxwell-type construction and let ρ_l and ρ_v be the corresponding saturated densities. In view of Eqs. (2.18) and (2.19) one sees that

$$\begin{aligned}\ln\frac{\mathcal{P}_N(\rho_l)}{\mathcal{P}_N(\rho_v)} &= -(\overline{f}_{{\rm can},l}-\overline{f}_{{\rm can},v}) + \tilde{\mu}_0(\rho_l-\rho_v) \\ &= \overline{p}_{{\rm can},l}-\overline{p}_{{\rm can},v} \\ &= 0. \end{aligned} \quad (2.20)$$

In other words, the peaks of the grand canonical density distribution that corresponds to the canonical choice of $\tilde{\mu} = \tilde{\mu}_0$, must be of equal height. While agreement between the various different ensembles is to be expected in the thermodynamic limit, this is not the case for finite (and small) systems.

In Fig. 1 we plot typical equal-height distributions for $L = 12\sigma$. Note that the temperature associated with curve (c) must be very close to an effective, finite-size canonical critical point $T^0_c(L)$ and likewise for the corresponding peak density $\rho^0_c(L)$. A better estimate of this finite-system critical point may be obtained by extracting the free-energy density numerically [cf. Eq. (2.18)] in the near-critical region and fitting the central region to a truncated Landau-type polynomial expansion, say,

$$\overline{f}_{\rm can}(\rho,\theta) = \sum_{j=0}^{J} A_j(\theta)\rho^j, \quad (2.21)$$

where $J \geqslant 4$. On using Eq. (2.19), the critical point is simply found by solving

$$\partial\tilde{\mu}_{\rm can}/\partial\rho = \partial^2\tilde{\mu}_{\rm can}/\partial\rho^2 = 0, \quad (2.22)$$

which represents the vanishing of the inverse compressibility.

Far below the critical region ($T \ll T_c$) when $\mu \simeq \mu_\sigma$, a grand canonical simulation encounters severe ergodicity problems owing to the large magnitude of the free-energy barrier that separates the two (meta)stable phases (peaks). The multicanonical preweighting scheme [35] utilizes a weighting function that forces the system to perform a close-to-uniform random walk throughout the entire density range of interest; this greatly facilitates the otherwise infrequent transitions between the two phases. However, an estimate of the weighting function is necessary; but that can be obtained recursively from a prior simulation at a higher temperature and subsequent histogram reweighting at the state of interest, or, alternatively, by utilizing general scaling properties of the distribution functions. The physical density distribution is obtained by dividing out the preweighting factors. We have employed this technique for $T \lesssim 0.95T^0_c(L)$.

C. Finite-size scaling theory

Finite-size scaling (FSS) theory [36, 37] was devised to describe the rounding and shifting effects that are invariably

observed in finite systems. In the context of magnetic systems characterized by a strong ordering field h and a weak ''temperaturelike'' field T, a property $Y(T,h)$ that exhibits a power-law type of divergence along the phase boundary or the symmetry axis $(h=0)$ in the thermodynamic limit, e.g.,

$$Y(T,h=0)\sim|t|^{-\omega}, \quad t=(T-T_c)/T_c, \tag{2.23}$$

is expected to scale as

$$Y(T,h,L)\approx L^{\omega/\nu}\tilde{Y}(tL^{1/\nu},hL^{\Delta/\nu}) \tag{2.24}$$

in the limit of large L. Here ν and $\Delta=\beta+\gamma$ are critical point exponents for the class of systems in question and $\tilde{Y}$ is a scaling function of universal form up to normalization of the variables. The scaling form (2.24) typically implies that (assuming $h=0$ for simplicity) a diverging quantity will reach a maximum value of height proportional to $L^{\omega/\nu}$. Moreover, the location of the maximum, which may be regarded as an effective critical point, say, $T_c^{(Y)}(L)$, should vary with the system size as

$$T_c^{(Y)}(L)-T_c(\infty)\approx Q^{(Y)}L^{-1/\nu}. \tag{2.25}$$

In the context of symmetric Ising or lattice-gas-type systems these finite-size scaling ideas have proven remarkably successful [38–43]. One simply determines the peak positions of the second- and higher-order derivatives of the free energy along the phase boundary in the field-temperature plane, or the symmetry axis $(h=0)$, for a series of increasing values of L and, assuming the correlation length exponent ν is known beforehand, subsequently extrapolates to the thermodynamic limit according to Eq. (2.25). On the other hand, the absence of any known symmetry axes in real fluid models makes FSS theory difficult to apply; one must locate the critical temperature T_c, the critical density ρ_c, and a locus corresponding in some sense to the symmetry axis $h=0$.

We have constructed and examined special loci—generally, defined by the inflection points of various properties—that enable us to compensate in a reasonable, systematic way for the absence of any known symmetry axes. A very natural choice is the line of inflection points of the density vs the chemical potential isotherms, i.e., $\rho=\rho(\tilde{\mu};\theta)$. Note that the inflection point is found by maximizing

$$\left(\frac{\partial\rho}{\partial\tilde{\mu}}\right)_\theta=\chi_{NN} \tag{2.26}$$

which, in other words [see Eq. (2.11)], means that one must solve the simple equation

$$\chi_{NNN}=0 \tag{2.27}$$

to determine the value of the chemical potential associated with the $\rho(\tilde{\mu})$ inflection point at a given fixed temperature (or coupling θ). In the thermodynamic limit $(L\to\infty)$ this locus must asymptotically approach the critical point although for finite L it will, in general, only pass near the critical point; see Fig. 2.

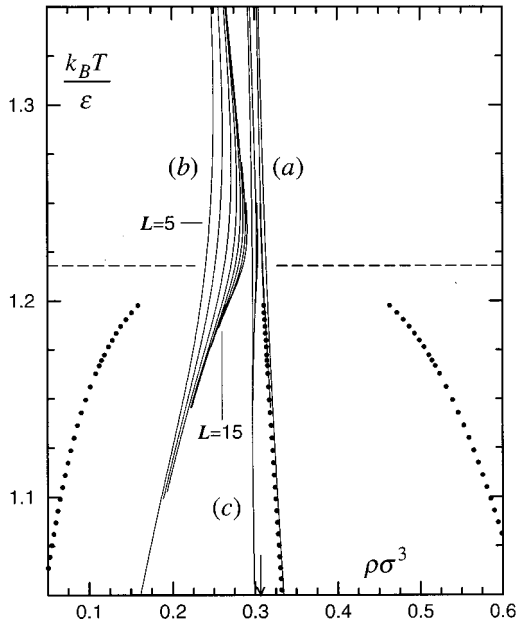

FIG. 2. Effective symmetry loci in the (T,ρ) plane as described in the text. The solid circles represent our estimates for the coexisting densities and the diameter. Curves (a) represent the $(\tilde{\mu},\rho)$ inflection locus, (b) the $(\overline{p},\rho)$ locus, and (c) the $\chi^{(1/4)}$ locus. Note that for (a) and (c) only the curves that correspond to $L/\sigma=5$, 10.5, and 15 are shown. For (b) the curves correspond from left to right to $L/\sigma=5$, 6, 7.5, 9, 10.5, 12, 13.5, and 15, respectively. The dashed horizontal line indicates the critical temperature $T_c(\infty)$. The arrow at the bottom indicates the estimate of the critical density $\rho_c(\infty)$.

Some noteworthy features about this $(\tilde{\mu},\rho)$ locus merit special attention. In the standard-lattice gas it coincides with the symmetry axis $(h=0)$ and the critical isochore—in other words the $\rho(\tilde{\mu})$ functional form is antisymmetric about the symmetry axis. This fact perhaps led Widom to formulate his original scaling equation of state in terms of (μ,ρ) variables [44]. On the experimental front, the point was examined in detail by Vicentini-Missoni *et al.* [45] for several simple fluids (such as CO_2, Ar, and He^4) and—although a real fluid possesses no known symmetry lines—it was concluded that the (μ,ρ) relationship was nearly antisymmetric about the critical isochore in the neighborhood of criticality.

Another natural choice of locus is the isothermal density-pressure or $(\overline{p},\rho)$ line of inflection points. As before, one finds for fixed temperature the value of chemical potential that maximizes

$$\left(\frac{\partial\rho}{\partial\overline{p}}\right)_\theta=\frac{1}{\rho}\left(\frac{\partial\rho}{\partial\tilde{\mu}}\right)_\theta=\frac{1}{\rho}\chi_{NN} \tag{2.28}$$

by solving

$$\chi_{NNN}-(\chi_{NN}^2/\rho)=0. \tag{2.29}$$

In a similar vein, one can investigate the locus of maxima of the isothermal fluid compressibility

$$\overline{K}_\theta = \frac{1}{\rho}\left(\frac{\partial \rho}{\partial \overline{p}}\right)_\theta = \frac{1}{\rho^2}\left(\frac{\partial \rho}{\partial \tilde{\mu}}\right)_\theta = \frac{1}{\rho^2}\chi_{NN}. \tag{2.30}$$

Finally, a more general ''*k* locus,'' which incorporates all the previous cases, can be defined by the maxima of the ''modified susceptibility''

$$\chi^{(k)} \equiv \chi_{NN}/\rho^k. \tag{2.31}$$

Then, as before, the corresponding value of the chemical potential, $\tilde{\mu}^{(k)}(T)$, is determined by solving

$$\chi_{NNN} - k(\chi_{NN}^2/\rho) = 0 \tag{2.32}$$

at temperature *T*. All the *k* loci are asymptotically critical in the sense that they spring from the true critical point when $L \to \infty$. It transpires that introducing the parameter *k* has the advantage of allowing one to approach the critical region from different directions: see Fig. 2.

Numerous further analogous possibilities might well be considered; for instance, one may define additional loci based on the constant-volume heat capacity, see Eq. (2.14) and Fig. 3. An additional locus—the ''canonical locus,'' $\tilde{\mu}^0_{\rm can}(T)$—may be defined by applying the equal-height criterion: see the discussion associated with Fig. 1 in Sec. II B. Since finite system criticality is classical along this locus, the standard methods used for every classical equation of state (e.g., van der Waals) may be used to locate a $T_c^0(L)$ and a $\rho_c^0(L)$: see the solid dots in Fig. 3. Of course, each corresponding locus, $\rho^0(T;L)$, *not* shown in Fig. 3, extends upwards only to $T_c^0(L)$.

The task of finite-size theory is now clear. In the context of precise simulations, one measures thermodynamic properties for a series of increasing system sizes *L*, over a range of temperatures along the previously defined ''pseudosymmetry'' axes, locates the appropriate peak positions, and extrapolates to the limit $L \to \infty$ according to Eq. (2.25) to estimate the infinite-volume critical temperature $T_c(\infty)$. The various properties, say Y_j, that we utilize constitute second- and higher-order derivatives of the grand potential and are conveniently defined in terms of density-energy moments.

Among the numerous possibilities, we have first considered the constant-volume heat capacity, $Y_1 = \check{C}_V$, defined by Eq. (2.14), as well as its constant-volume derivative, $Y_2 = (\partial \check{C}_V/\partial\theta)_\rho$, which is found using Eq. (2.13). In accord with studies in magnetic systems [19], the heat capacity is found to have a maximum—thereby defining $T_1(L)$—below the critical temperature, while its derivative has two local extrema at $T_2^+(L)$ and $T_2^-(L)$, respectively.

Additional estimators may be defined in terms of the behavior of the derivatives of the order parameter $M = \delta N = N - \langle N \rangle$. These yield the estimators

$$Y_3 = \frac{1}{V}\left[\frac{\partial \langle |M| \rangle}{\partial \theta}\right]_\zeta, \quad Y_4 = \frac{1}{V}\left[\frac{\partial \langle M^2 \rangle^{1/2}}{\partial \theta}\right]_\zeta, \tag{2.33}$$

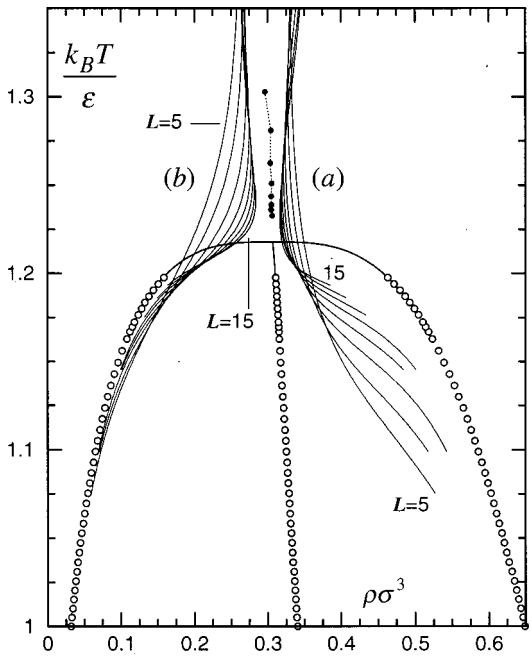

FIG. 3. Maximum heat-capacity lines in the (T, ρ) plane. The curves labeled (a) correspond to the maxima of the heat capacity density $\check{C}_V$ as defined in Eq. (2.14). Curves (b) denote the maxima of the heat capacity per particle, $\check{C}_V/\rho$. All system sizes ($L/\sigma = 5$, 6, 7.5, 9, 10.5, 12, 13.5, and 15) are shown for both (a) and (b). The saturated densities and the diameter are represented by open circles; the solid lines that emanate from the open circles are based on an Ising-type fit: see text in Sec. III. The filled circles denote the finite-system $[T_c(L), \rho_c(L)]$ locus that is obtained from the canonical free-energy density—derived from grand canonical data—by fitting to a fourth degree polynomial and evaluating the critical point classically for every *L*.

$$Y_5 = \frac{1}{V}\left[\frac{\partial \langle M^4 \rangle^{1/4}}{\partial \theta}\right]_\zeta, \quad Y_6 = \frac{1}{V}\left[\frac{\partial \langle M^6 \rangle^{1/6}}{\partial \theta}\right]_\zeta, \tag{2.34}$$

respectively. Here the subscript ζ stands for the locus under consideration, e.g., the *k* locus derived from $\chi^{(k)}$. Following our previous work [19], we have also defined the Ising-type susceptibilities

$$\check{\chi}_2 \equiv Y_7 = \frac{1}{V}[\langle M^2 \rangle - \langle |M| \rangle^2], \tag{2.35}$$

$$\check{\chi}_4 \equiv Y_8 = \frac{1}{V}[\langle M^4 \rangle - 4\langle |M| \rangle \langle |M|^3 \rangle + 12\langle M^2 \rangle \langle |M| \rangle^2 - 3\langle M^2 \rangle^2 - 6\langle |M| \rangle^4]. \tag{2.36}$$

Note that $\check{\chi}_4(T)$ exhibits two extrema (on a locus ζ), say, $T_8^+(L)$ and $T_8^-(L)$, respectively.

Last but not least, estimators based on the so-called Binder parameter and variants [32, 38, 41, 43] can also be considered. To that end we have opted to examine

$$Y_9 = \frac{\partial}{\partial \theta}\left[\frac{\langle M^4 \rangle}{\langle M^2 \rangle^2}\right]_\zeta, \quad Y_{10} = \frac{\partial}{\partial \theta}\left[\frac{\langle M^2 \rangle}{\langle |M| \rangle^2}\right]_\zeta, \tag{2.37}$$

$$Y_{11}=\frac{\partial}{\partial\theta}\left[\frac{\langle M^4\rangle}{\langle|M|\rangle^4}\right]_\zeta, \quad Y_{12}=\frac{\partial}{\partial\theta}\left[\frac{\langle M^6\rangle}{\langle|M|\rangle^6}\right]_\zeta. \tag{2.38}$$

Needless to say, there are many more combinations that one can construct such as, for instance, estimators based on $\delta U=U-\langle U\rangle$. However, as we will see below, the set Y_j for $j=1,\ldots,12$, together with the canonical loci (labeled 0) will amply suffice for the present investigation. The infinite-volume critical temperature $T_c(\infty)$ is obtained from Eq. (2.25) by extrapolating the peak positions, $T_c^{(Y_j)}(L;\zeta)$ say, towards the thermodynamic limit. Once the critical temperature has been reliably established, an L-dependent pseudocritical density, $\rho_c(L,T_c(\infty);\zeta)$, may be calculated for the locus ζ under consideration and the process is repeated for the whole set of the loci. The infinite-system critical density $\rho_c(\infty)$ is estimated by extrapolation of these various locus-dependent density approximants towards $L=\infty$. The procedure will be demonstrated explicitly in the next section.

III. THE CRITICAL REGION OF THE SQUARE-WELL FLUID

In accord with the approach explained above, we have performed grand canonical Monte Carlo simulations for the HCSW fluid for system sizes $L/\sigma=5$, 6, 7.5, 9, 10.5, 12, 13.5, and 15. For a given temperature the chemical potential was chosen—through histogram reweighting—so as to yield an average density of $\rho^*=\rho\sigma^3\simeq 0.3$, a value close to the previous best estimates of the critical density [7,46–48]. For low temperatures, a relatively few multicanonical simulations [35] were carried out to facilitate transitions between the low- and high-density phases. For higher temperatures, additional simulations were performed at chemical potentials designed to sample densities somewhat below and somewhat above ρ_c. The total length of each simulation was in the range of $20-80\times 10^6$ trial configurations per unit volume (σ^3), depending on the particular system size L under investigation. The data were stored in two-dimensional energy-density histograms with bins of size $\Delta N=1$ and $\Delta U=2n-1$ ($n\geqslant 1$). The different loci explained in the preceding section were found through histogram reweighting. The properties Y_j were measured along these lines as a function of the reduced inverse temperature θ and the corresponding peak positions $\theta_j(L;\zeta)$ were determined.

The exponent ν, governing the divergence of the correlation length ξ, was found by the unbiased method described in [19] and tested there for symmetric magnetic systems. One considers the peak positions $\theta_j(L)$ and $\theta_k(L)$ for a pair of properties Y_j and Y_k, and forms the ratio

$$y_{jk}=\left[1-\frac{\theta_j(L+\delta L)-\theta_k(L+\delta L)}{\theta_j(L)-\theta_k(L)}\right]\frac{L+l_0\sigma}{\delta L}. \tag{3.1}$$

It is expected that $y_{jk}\to 1/\nu$ when $L\to\infty$. The small adjustable shift parameter l_0 partially compensates for the inevitable corrections to leading-order scaling.

In Fig. 4 the behavior of y_{jk} along the $(\tilde{\mu},\rho)$ locus is examined vs $1/L$ for the HCSW fluid for two pairs of properties and various values of the shift l_0. The data appear to extrapolate to the neighborhood of the expected Ising limit $\nu\simeq 0.63_0$ [20] when $L\to\infty$, although the precision is not as good as in the magnetic models of [19]. By examining a set of similar plots using other pairs of properties Y_j and Y_k and different loci, all displaying essentially similar behavior, we conclude

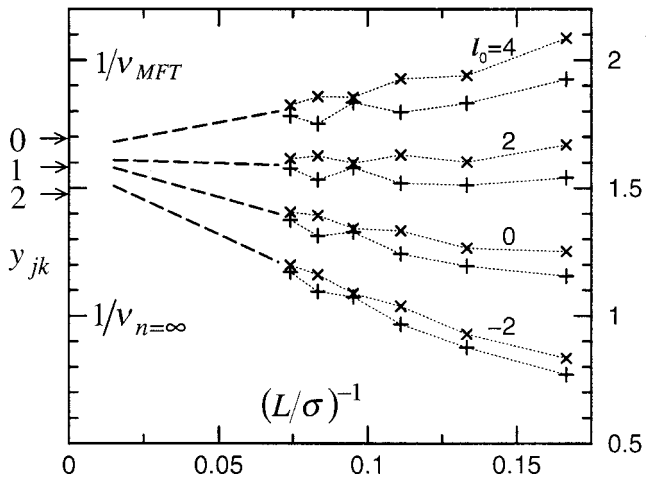

FIG. 4. Estimation of the inverse correlation length exponent $1/\nu$ for the HCSW fluid using the estimators y_{jk} defined in Eq. (3.1). The crosses ($\times$) correspond to the pair $(Y_{12},Y_8^{(-)})$ whereas the plusses (+) derive from $(Y_{12},Y_8^{(-)})$. Both pairs were taken along the $(\tilde{\mu},\rho)$ inflection locus ($k=0$). The arrows on the ordinate indicate, from the highest downwards, estimates of $1/\nu$ for $n=0$ (self-avoiding walks), $n=1$ (Ising), and $n=2$ (XY) systems [20]. The values $1/\nu=2$ and 1 correspond to mean-field theory and the spherical model ($n=\infty$) [49], respectively. The parameter l_0 represents a shift ($L\Rightarrow L+l_0\sigma$) that is merely an aid to extrapolation [19]: see also Eq. (3.1).

$$\nu_{\mathrm{HCSW}}=0.63\pm 0.03. \tag{3.2}$$

Although one might wish for higher precision, it is clear that significantly longer and larger simulations would be needed to do much better. Nevertheless, this estimate serves, as mentioned, to distinguish the HCSW fluid from self-avoiding walks with $\nu\simeq 0.58_8$ and XY spin systems with $\nu\simeq 0.67_6$ [20].

The next step involves the determination of the critical temperature by extrapolating the peak positions $k_BT_j(L)/\varepsilon=1/\theta_j(L)$ to the $L\to\infty$ limit according to Eq. (2.25). To this end we will accept the central, Ising estimate $\nu=0.630$ from here on. In Fig. 5 we present this extrapolation on the chemical potential-density inflection locus: we thence conclude

$$T_c^*\equiv k_BT_c(L)/\varepsilon=1.2179\pm 0.0003, \tag{3.3}$$

which closely matches the precision achieved in [19] for magnetic systems. Examination on different loci leads to the same estimate since the peak positions for a particular quantity Y_j prove rather insensitive to the particular choice of locus (in the range $k=0$ to 1).

As already mentioned, once the critical temperature has been established, the critical density can be found most simply by recording the values of $\rho_c(L,T_c(\infty);\zeta)$ for several loci ζ and a sequence of system sizes L. Extrapolation to the limit

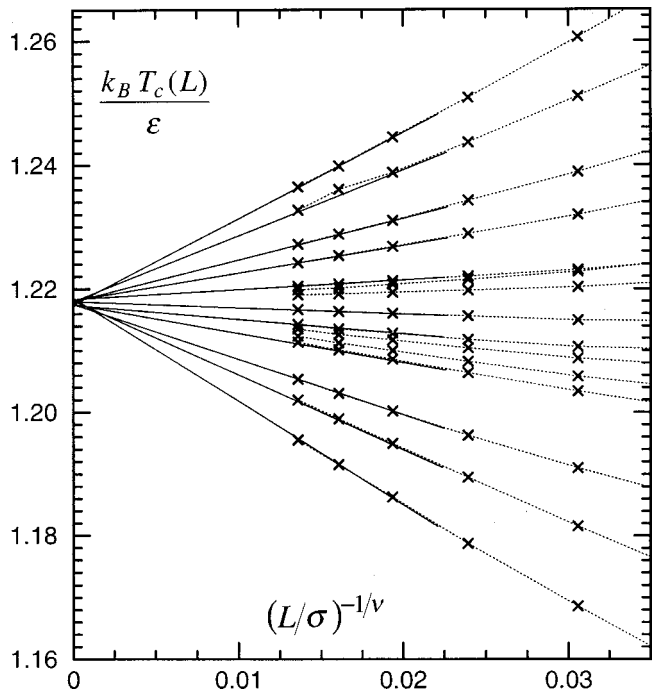

FIG. 5. Critical temperature estimation for the HCSW fluid by extrapolation to the $L\to\infty$ limit. A value of $\nu=0.630$ has been assumed. The highest line corresponds to Y_{12}. The second highest line represents the canonical critical points $T_c^0(L)$: see text and, in particular, Fig. 3. From the third highest downwards the lines correspond to properties Y_j for $j=10$, $2^{(+)}$, $7^{(+)}$, 9, 6, 5, 4, 3, 1, $7^{(-)}$, and $2^{(+)}$, respectively. All lines except the second highest have been obtained on the $(\tilde{\mu},\rho)$ (or $k=0$) inflection locus.

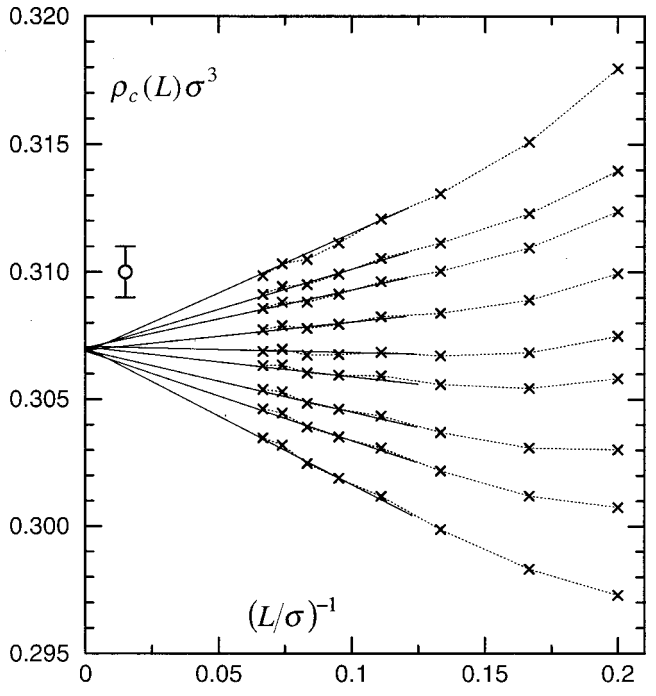

FIG. 6. Critical density estimation for the HCSW fluid by extrapolation to $L\to\infty$. The highest line represents $\rho_c^{(0)}(L)$ obtained from the canonical coexistence locus at $T_c(\infty)$. The remaining curves correspond to different $\chi^{(k)}$ loci evaluated at the estimate for $T_c(\infty)$. From the second highest line downwards the associated values of k are 0, $\frac{1}{40}$, $\frac{1}{16}$, $\frac{1}{10}$, $\frac{1}{8}$, $\frac{1}{6}$, $\frac{1}{5}$, and $\frac{1}{4}$, respectively. The open circle denotes the (infinite-volume) estimate obtained in Ref. [7] using the Bruce-Wilding approach [25, 26].

of infinite system size can then be performed as illustrated in Fig. 6. It should be noted, however, that the exponent of the asymptotic approach is open to debate: see remarks in Sec. IV. We decided to extrapolate vs $1/L$ and thus obtain an estimate free of assumptions as to further exponent values. We may note that separate sets of estimators, say, $\rho_c^{(k)}(L)$, may be obtained from the individual k loci, since these display well-defined extrema as a function of T: see the plots in Fig. 2 and, likewise, in Fig. 3. Behavior comparable to Fig. 6 is observed but the data are not quite as precise and smooth numerically as those obtained from the fixed isotherm $T=T_c(\infty)$. Overall we conclude

$$\rho_c^*\equiv\rho_c\sigma^3=0.3067\pm0.0004. \tag{3.4}$$

This estimate which, evidently, is based on a systematic study of a range of approximants, is roughly an order of magnitude more precise than that of [7] based on the Bruce-Wilding method [25, 26]: see Fig. 6. Furthermore, the earlier estimate seems subject to distinct bias.

Our grand canonical results for the coexisting densities for the HCSW fluid are shown as solid black circles in Fig. 7: see also Fig. 2 for the data at lower temperatures. The open circles that lie within the two-phase region correspond to maxima of the heat capacity, $\check{C}_V(T,\rho;L)$, obtained along a line of fixed mean density, i.e., on an isochore. Note that for $\rho\neq\rho_c$, the heat capacity in the thermodynamic limit jumps discontinuously on crossing the phase (or saturation) boundary; however, the finite-system heat capacity will inexorably exhibit a rounded maximum or peak depending explicitly on L. In the same figure we also show the finite-L ''canonical'' coexistence curves that follow from the equal-height procedure explained in Sec. II B. Evidently, these values all lie in the (limiting) single-phase region.

As in other cases [7,17], reliable grand canonical results do not reach the close-to-critical region; thus no direct estimate for the phase boundary is possible in the range $0.15\lesssim\rho\sigma^3\lesssim0.45$. In order to obtain some reasonable estimate or bound for the saturation temperature, $T_s(\rho)$ say, in this ''inner region'' where no direct values are available, we have attempted to extrapolate the canonical saturation temperatures, $T_s^{(\mathrm{can})}(\rho;L)$, and the heat-capacity maxima, $T_s^{(C_V)}(\rho;L)$, to the limit of infinite size. Note that these two different estimators approach the thermodynamic limit from opposite directions so that weighted averages converge more rapidly and plots vs $1/L$ are informative, although they exhibit systematic curvature that is hard to extrapolate with full conviction (except for $\rho\simeq\rho_c$ when plots vs $1/L^{1/\nu}$ become linear). Note, indeed, that for $\rho\neq\rho_c$ and *large enough* values of L, finite-size scaling theory indicates that the convergence should be *exponentially fast* in L. However, it is clear from Fig. 7 that such a regime is not accessible in our simulations: rather, some crossover dependence on L is realized for $\rho\neq\rho_c$. Despite these caveats, judicious extrapolation yields

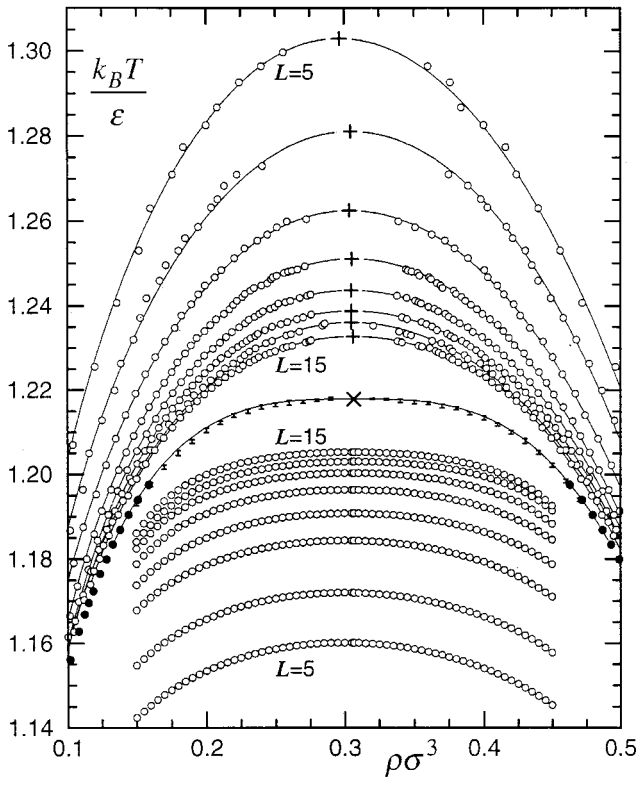

FIG. 7. Coexisting densities for the HCSW fluid. The black circles represent direct grand canonical estimates. The position of the critical point is indicated by the cross (×). The solid line that emanates from the solid circles is a simple Wegner-type fit: see Eqs. (3.5) and (3.6). The open circles in the two-phase region locate finite-L heat-capacity maxima along a locus of fixed density. The open circles that lie above the solid circles and the Wegner-type fit represent the finite-L canonical estimates: see Sec. II B. The plusses (+) represent the (finite-L) canonical critical points $T_c^0(L)$, $\rho_c^0(L)$. The solid lines connecting the canonical orthobaric densities with their associated critical point represent classical van der Waals fits. The error bars lying close to the Wegner fit indicate estimated bounds for the saturation temperature for a given fixed orthobaric density: see text.

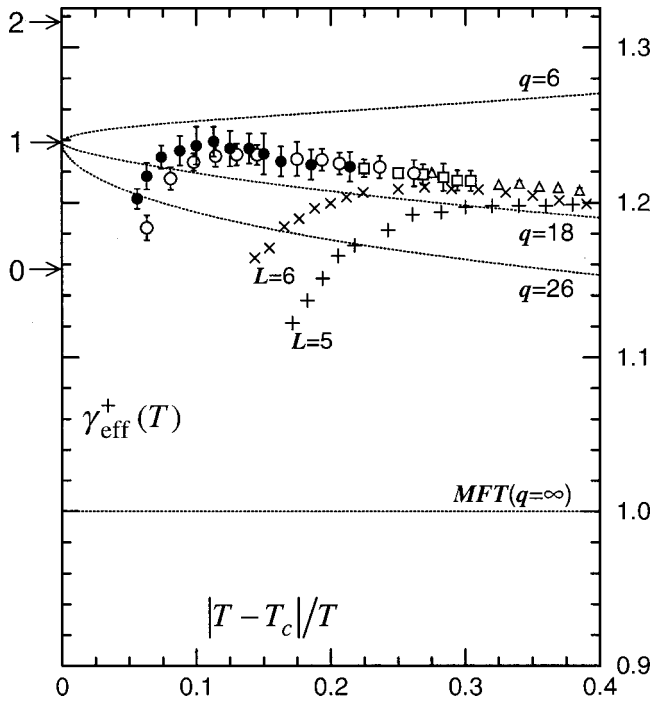

FIG. 8. Effective high-temperature susceptibility exponent, $\gamma_{\rm eff}^+(T)$, along the critical isochore for the HCSW fluid with $\lambda = 1.5$ for sizes denoted: (+) $L=5$; (×) $L=6$; (△) $L=7.5$; (□) $L=9$; (○) $L=10.5$; (●) $L=12$, all in units of σ. Note that for intermediate L the finite-size-induced falloff of $\gamma_{\rm eff}^+$ as $T \to T_c$ has been omitted for clarity. The horizontal arrows indicate the values of γ for the $n=0$, 1, and 2 universality classes [20]. The dotted lines that approach the $n=1$ limit derive from series expansion data for Ising models with first ($q=6$), first-plus-second ($q=18$), and first-plus-second-plus-third ($q=26$) equivalent-neighbor interactions: see [19]. The horizontal line at $\gamma_{\rm eff}^+=1$ represents the Curie-Weiss or mean-field-theory result for the Ising model; this corresponds to $q \to \infty$.

the quite closely spaced upper and lower estimates for $T_s(\rho)$ presented as error bars in Fig. 7.

To supplement these results we have fitted the grand-canonical coexistence data (solid dots in Figs. 7 and 2) to the truncated Wegner-type expansions (see [1])

$$[\overline{\rho}(T)-\rho_c]\sigma^3 \simeq a_{2\beta}|t|^{2\beta}+a_{1-\alpha}|t|^{1-\alpha}+a_1 t, \qquad (3.5)$$

where the diameter is defined in Eq. (1.3) and

$$[\rho_{\rm liq}(T)-\rho_{\rm vap}(T)]\sigma^3 \simeq B|t|^{\beta}[1+b_\theta|t|^{\theta}+b_{2\beta}|t|^{2\beta}]. \qquad (3.6)$$

For the purpose of fitting we have adopted the Ising values $\beta=0.326$, $\alpha=0.109$, and $\theta=0.52$ [1, 20]. We find a good fit with $B=1.2026_4$, which we believe represents a reasonable estimate of the true limiting amplitude, and $a_{2\beta}=-0.0007_3$, $a_{1-\alpha}=0.189_7$, $a_1=-0.0691_4$, $b_\theta=-0.257_6$, and $b_{2\beta}=-0.085_2$. It must be emphasized, however, that *no* significance should be attached to the specific numerical values of the five correction coefficients since, without doubt, higher-order corrections must be playing a non-negligible role in the wide range fitted. Furthermore, because the exponents appearing differ rather little in magnitude, the fitting uncertainties will be strongly correlated. The fit (3.6) to the coexistence curve is shown in Fig. 7 as a solid line that connects the coexisting densities (solid circles) to the critical point. Judging by the close proximity of the fit to the fixed-density estimates, we conclude that our extrapolations provide reasonably reliable values although much bigger sizes are needed to obtain higher resolution at near critical densities.

Given a reliable estimate of the critical point, one may measure a miscellany of quantities that characterize the approach to criticality and elucidate possible crossover scenaria: potentially the most revealing examples are the effective exponents. The effective high-temperature susceptibility exponent, defined by

$$\gamma_{\rm eff}^+(\theta;\zeta) = -(\partial \ln \chi_{NN}/\partial \ln|t'|)_\zeta, \qquad (3.7)$$

is the most readily obtainable quantity. Here we employ $t' = |T - T_c|/T$ while ζ is a critical locus asymptotically tangent to the phase boundary $\tilde{\mu}_\sigma(T)$. The limiting value of $\gamma^+_{\rm eff}$ is the exponent γ that dictates the asymptotic power-law divergence of the susceptibility χ_{NN}. The most obvious choice for the locus ζ is the critical isochore $\rho = \rho_c$, as invariably used in experiments; other choices are, however, feasible. Following Sec. II A, one obtains (for the critical isochore)

$$\gamma^+_{\rm eff}(\theta;\rho_c) = (\theta_c - \theta)\left(\chi_{NNN}\frac{\chi_{NU}}{\chi^2_{NN}} - \frac{\chi_{NNU}}{\chi_{NN}} \right), \qquad (3.8)$$

where the various second- and third-order susceptibilities are defined in Eq. (2.10) and are evaluated for the values of the chemical potential $\tilde{\mu}(T)$ that correspond to ρ_c. Our estimates for $\gamma^+_{\rm eff}(T)$ on the critical isochore are reproduced in Fig. 8. The full rounding effects are indicated only for some of the system sizes considered to avoid cluttering the figure. The uncertainty bars in Fig. 8 were computed by breaking the full simulations into five to ten subsimulations. The values of $\gamma^+_{\rm eff}$ are not as smooth as our previous estimates for symmetric Ising-type systems [19]. Indeed, while for the Ising lattice gases the simulations were performed along the *known* symmetry axis—which, *inter alia*, coincides with the critical isochore—the uncertainties in determining the locus $\rho = \rho_c$ as well as the uncertainty in ρ_c itself must be taken into consideration for an asymmetric fluid model. Nevertheless, on extrapolating the values shown in Fig. 8, we conclude

$$\gamma_{\rm HCSW} = 1.245 \pm 0.025, \qquad (3.9)$$

which distinguishes the HCSW fluid unmistakably from the $n=0$ and $n=1$ universality classes [49], with $\gamma_{\rm saw} \simeq 1.15_9$ and $\gamma_{\rm XY} \simeq 1.31_6$, respectively [20], and comfortably encompasses the Ising value $\gamma = 1.23_9$ [20].

It is interesting to note from Fig. 8 that $\gamma^+_{\rm eff}(T)$ approaches the limit γ from *below* as $T \to T_c+$. This behavior characterizes most real, simple fluids like CO_2, but differs from the nearest-neighbor simple cubic lattice gas for which $\gamma^+_{\rm eff}(T)$ is described by the dotted line labeled $q=6$ in the figure. Indeed, in terms of the equivalent-neighbor lattice-gas results labeled by the coordination numbers $q=18$ and 26 [19] in Fig. 8, the HCSW fluid for $\lambda = 1.5$ would appear to correspond roughly to a lattice gas with, say, $q=10$ to 14 equivalent-neighbor couplings.

The effective exponent that describes the shape of the coexistence curve may be defined by

$$\beta_{\rm eff}(\theta) = (d\ln[\Delta\rho(T)]/d\ln|t'|), \qquad (3.10)$$

where the width of the coexistence curve is $\Delta\rho(T) = \rho_{\rm liq} - \rho_{\rm vap}$. Note that the associated orthobaric densities, $\rho_{\rm liq}(T)$ and $\rho_{\rm vap}(T)$, are shown as solid circles in Fig. 7 and, down to lower temperatures, in Fig. 2. The points plotted in Fig. 9 represent our estimates of $\beta_{\rm eff}$ derived by numerical differentiation of the $\Delta\rho(T)$ estimates on a $\ln|t'|$ plot. The data closest to T_c (arising from the $L = 15\sigma$ simulation) show signs of a sharp upturn which we believe is primarily a result

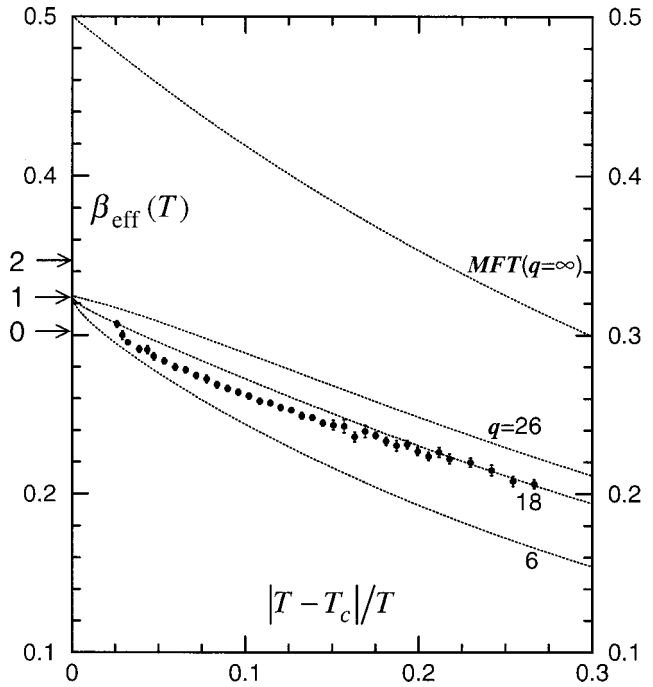

FIG. 9. Effective coexistence curve exponent, $\beta_{\rm eff}(T)$, for the HCSW fluid (solid circles) derived as explained in the text. The dotted lines and the arrows have the same meaning as in Fig. 8.

of the onset of finite-size rounding. Allowing, with reasonable prudence for the statistical and systematic errors, leads us to conclude

$$0.304 \leqslant \beta_{\rm HCSW} \leqslant 0.340. \qquad (3.11)$$

The confidence limits here are fully consistent with the previously quoted Ising value $\beta = 0.32_6$ but barely exclude the self-avoiding-walk ($n=0$) and XY($n=2$) values, namely, 0.30_2 and 0.34_7, respectively [20], which, however, are rather closely spaced. As for $\gamma^+_{\rm eff}$, the approach to criticality corresponds to an equivalent-neighbor lattice gas with an effective coordination number lying within the range $q=8$ to 16.

Note that no sign of crossover from some mean-field-type behavior is suggested by the variation of either $\gamma^+_{\rm eff}(T)$ or $\beta_{\rm eff}(T)$, but, of course, none is expected since the HCSW fluid with $\lambda = 1.5$ represents a short-range interaction potential. For larger values of λ this must change, but it would seem that the results to be anticipated could be read off fairly well from the previous extensive studies of long-range crossover in the lattice systems [21–23].

In our study of the lattice gases [19] we were able to check behavior corresponding to the Ising universality class further by examining $\gamma^-_{\rm eff}(T)$, for the susceptibility below T_c, and also by estimating the corresponding amplitude ratio C^+/C^- [19, 50]. Unfortunately, the range of sizes and statistical precision available to us for the hard-core square-well fluid precludes these tests. However, we believe that the data and analyses presented for the $\lambda = 1.5$ model leave no serious room for doubt that the Ising universality class describes this continuum model.

IV. INVESTIGATION OF THE YANG-YANG ANOMALY

In 1964 Yang and Yang [2] pointed out that the total constant-volume heat capacity $\mathcal{C}_V^{\rm tot}$ of a single-component fluid can be decomposed into two terms, one derived from the variation of the pressure p, the other from the chemical potential μ: explicitly one has

$$\mathcal{C}_V^{\rm tot} = VT(\partial^2 p/\partial T^2)_V - NT(\partial^2 \mu/\partial T^2)_V . \qquad (4.1)$$

On the other hand, it is well established that on approaching the critical point—along, say, the critical isochore—the heat capacity exhibits a weak singularity, $\mathcal{C}_V^{\rm tot} \sim |t|^{-\alpha}$, with, accepting the Ising value [1, 20], $\alpha = 0.109 \pm 0.004$. This implies that *either* the pressure term *or* the chemical potential term in Eq. (4.1), or perhaps *both*, must diverge when $T \to T_{c^-}$ along the vapor pressure curve $p_\sigma(T)$ or, equivalently, along the phase boundary $\mu_\sigma(T)$. In the standard lattice gas, the chemical potential on the phase boundary is a simple, analytic function of the temperature. This is, indeed, also the case for the special asymmetric model fluids with a hidden symmetry of [3–5]. In these systems, therefore, $(d^2 p_\sigma/dT^2)$ diverges like $C_V(T,\rho_c)$ but $(d^2\mu_\sigma/dT^2)$ remains bounded. Early analyses of two-phase specific-heat data for water [45, 51] seemed to support this scenario. However, the data were not sufficiently precise to draw reliable conclusions: see the discussion in [6].

On the other hand, recent analysis [1, 6] of extensive two-phase specific-heat data for propane [52] and a previous study of CO_2 [53] demonstrated the contrary: the heat-capacity singularity is, in fact, *shared* between the two terms on the right-hand side of Eq. (4.1). It was found [1, 6] that when $T \to T_{c^-}$, the second derivative of $\mu_\sigma(T)$, say μ_σ'', diverges to $-\infty$ for propane but to $+\infty$ for CO_2. Regarding the strength of this ''Yang-Yang (Y-Y) anomaly,'' it was concluded [1, 6] that the chemical potential term is responsible for about 56% of the total C_V singularity in propane below T_c. For the case of CO_2, the associated ratio R_μ was estimated, with lower precision, to be roughly -0.35. Note that the negative value implies that the pressure contribution actually diverges faster than C_V itself, by virtue of having a larger critical amplitude.

The consequences of the Yang-Yang anomaly for a scaling description of fluids have been discussed in [1, 5]. Owing to the appearance of the pressure—not previously expected—in the fluid scaling-field variables, the coexistence diameter (1.3) gains a dominant $|t|^{2\beta}$ term. In the context of simulations, the mixed-field finite-size scaling theory of Bruce and Wilding [25, 26]—currently the state of the art approach for asymmetric fluids—precludes the occurrence of a Yang-Yang anomaly. This fact, indeed, provided one of the motivations for the present (unbiased) finite-size investigation.

It is appropriate, conversely, to point out here that the presence of a Y-Y anomaly in the HCSW or other model fluid may significantly undermine the validity of the finite-size extrapolations used in the Bruce-Wilding approach to estimate the critical density ρ_c [25,26]. In particular, in their analog of Fig. 6, Bruce and Wilding specifiy a particular inverse power of the size L related to the fact that pure (μ, T) scaling-field mixing introduces only a correction term $|t|^{1-\alpha}$ into the diameter (and elsewhere); but, as mentioned, when pressure mixing occurs, the more singular term $|t|^{2\beta}$ also appears as, e.g., in Eq. (3.5) [1]. It seems likely, therefore, that in the appropriate adaptation of the Bruce-Wilding ''fixed-point-distribution matching'' procedure, some other inverse powers of L will enter—quite possibly in a competing manner. This is why, in Fig. 6, we adopted an agnostic point of view and simply plotted vs $1/L$. Insofar as there is some residual curvature in the plots—which is certainly hard to see—some other power or combination of powers of L could be present. However, the use of a large number of *distinct* approximating sequences allows one to extrapolate with confidence even though the true asymptotic form may remain obscure.

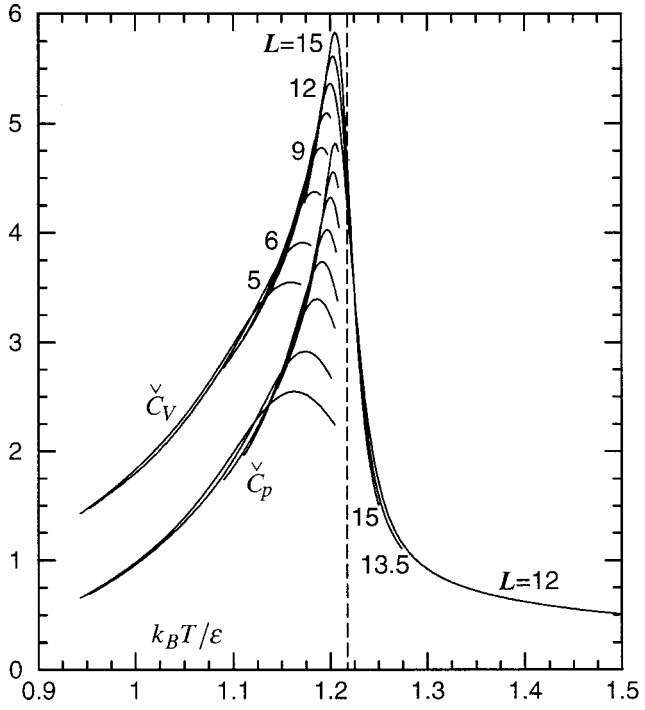

FIG. 10. The reduced heat-capacity density $\check{C}_V(T)$ and the corresponding pressure contribution $\check{C}_p(T)$ [defined in Eqs. (2.14) and (4.2)] calculated on the critical isochore for the HCSW fluid. Note that some of the extensions into the one-phase region have been truncated for reasons of clarity.

For our study of the Y-Y anomaly in the HCSW fluid, we have employed a slightly different version of Eq. (4.1)—albeit with the same implications—namely, in terms of the $(\overline{p}, \tilde{\mu}, \theta)$ variables

$$\check{C}_V = \left(\frac{\partial^2 \overline{p}}{\partial \theta^2}\right)_\rho - \rho\left(\frac{\partial^2 \tilde{\mu}}{\partial \theta^2}\right)_\rho \equiv \check{C}_p(\theta,\rho) + \check{C}_\mu(\theta,\rho), \quad (4.2)$$

where $\check{C}_p = (\partial^2 \overline{p}/\partial\theta^2)_\rho$ and $\check{C}_\mu = -\rho(\partial^2\tilde{\mu}/\partial\theta^2)_\rho$. Recall that the heat-capacity density, $\check{C}_V(\theta,\rho)$, is defined in Eq. (2.14). The chemical potential term can be expressed readily, using Eq. (2.13), in the form

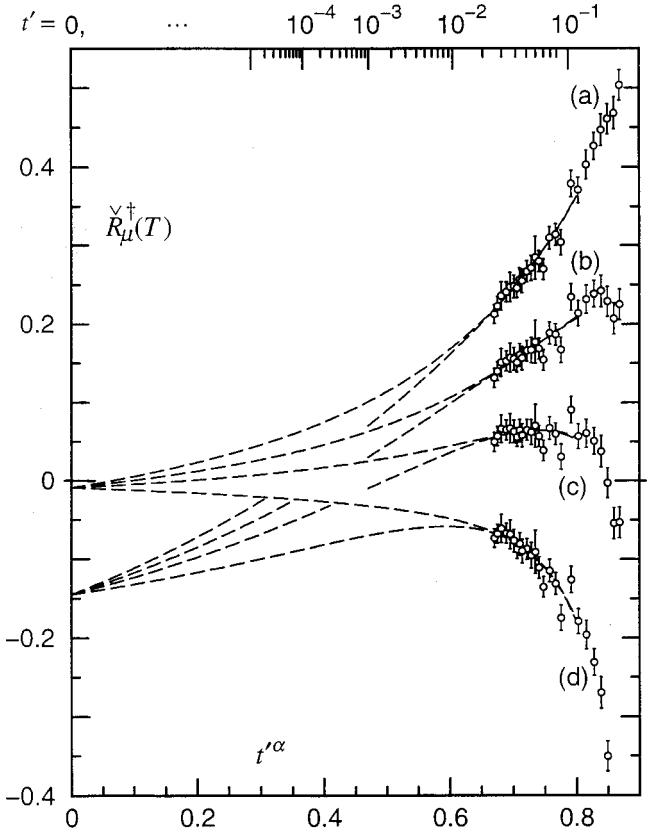

FIG. 11. Estimation of the strength R_μ of the Yang-Yang anomaly for the HCSW fluid with $\lambda = b/\sigma = 1.5$ via plots of $\check{R}_\mu^\dagger(T;B^\dagger)$ [as defined in Eq. (4.4)] vs t'^α with $t' = 1-(T_c/T)$. The data pertain to $\rho = \rho_c$ and $T < T_c$. The dashed curves have been derived from separate fits to selected simulation data for $\check{C}_V(T)$ and $\check{C}_p(T)$: see text. Cases (a), (b), (c), and (d) correspond to ''background shifts'' $B^\dagger = 0$, 0.4, 0.8, and 1.4, respectively.

$$\left(\frac{\partial^2 \tilde{\mu}}{\partial \theta^2}\right)_\rho = 2\frac{\chi_{NU}\chi_{NNU}}{\chi_{NN}^2} - \frac{\chi_{NU}^2\chi_{NNN}}{\chi_{NN}^3} - \frac{\chi_{NUU}}{\chi_{NN}}. \quad (4.3)$$

Finally, the pressure term may be found simply from Eq. (4.2) via $\check{C}_p = \check{C}_V - \check{C}_\mu$. Note that owing to the complex expression for $\check{C}_\mu$ in Eq. (4.3) and the inextricable presence of almost cancelling third-order moments, a sufficiently delicate finite-scaling analysis might well lie beyond current computational resources. In addition, one must remember that a weak $|t|^{-\alpha}$ singularity is always accompanied by relatively strong analytic terms—usually known as ''background.'' This typically bedevils the unambiguous elucidation of the singularity. Last but not least, the overall amplitude of the asymptotic $|t|^{-\alpha}$ term in $\check{C}_\mu$ may itself be small for the HCSW fluid since the strength of Y-Y anomalies seems to be related to the asymmetry of the constituent molecules: see [1] and [6].

We have calculated $\check{C}_V$ and $\check{C}_p$ along the critical isochore, $\rho = \rho_c$ for sizes $L/\sigma = 5$ to 15: see Fig. 10 [54]. Over the accessible size range it is evident that $\check{C}_p(T;\rho_c)$ is always smaller than $\check{C}_V(T,\rho_c)$; but it appears to rise somewhat more sharply as $T \to T_c-$. This behavior is strongly reminiscent of the observations of CO_2, where the pressure contribution exceeds that of the heat capacity only for $|t'| \lesssim 0.005$. To estimate the strength R_μ of a possible Yang-Yang anomaly in the HCSW fluid, we adopt the procedures developed to analyze propane and CO_2 [1,6] and so define the dimensionless ratio

$$\check{R}_\mu^\dagger(T) \equiv \frac{\check{C}_\mu(T,\rho_c) - B^\dagger}{\check{C}_V(T,\rho_c)}, \quad (4.4)$$

where $B^\dagger$ is a constant ''background shift'' introduced as an aid to extrapolation to T_c-. Note, indeed, that $\check{R}_\mu^\dagger(T)$ has the same limit $R_\mu \equiv \lim_{T\to T_c-} \check{R}_\mu^\dagger(T)$, irrespective of the particular value of the shift $B^\dagger$.

In Fig. 11 we plot the function $\check{R}_\mu^\dagger$ vs t'^α for a selected set of data away from the rounding regions below T_c (see Fig. 10) and for four different values of $B^\dagger$. It is important to realize that $\check{R}_\mu^\dagger(T)$ should approach its asymptotic value *linearly* in terms of t'^α (except for one special choice of $B^\dagger$ for which the approach may be *more* rapid) [1,6]. The dashed lines in Fig. 11 represent the results of fits to $\check{C}_V(T,\rho_c)$ and $\check{C}_p(T,\rho_c)$, respectively, based on the form

$$\check{C}(T) = A|t'|^{-\alpha}(1 + a_\theta|t'|^\theta) + B_0 + B_1 t, \quad (4.5)$$

which allows for a correction-to-scaling term with exponent $\theta = 0.52$ (as accepted in Sec. III [20]) and for two background terms. The quality of our data do not, in fact, allow sensible fits with more than three terms. Accordingly, we display in Fig. 11, first, the consequences of setting $B_1 = 0$ in Eq. (4.5) (for both $\check{C}_V$ and $\check{C}_p$) which yields $R_\mu \simeq -0.145$ (i.e., the lower set of fits) and then of setting $a_\theta = 0$ which leads to the upper set of fits with $R_\mu \simeq -0.009$. Excluding the two and four selected data points closest to T_c does not change these fits qualitatively. The average of the two fits to $\check{C}_V$ and $\check{C}_p$, which we prefer since the a_θ term dominates over the B_1 term for small t, yields $R_\mu \simeq -0.071$.

The undesirable scatter of the data for $\check{R}_\mu^\dagger(T)$ in Fig. 11 is evidently due to the increasing difficulty of obtaining accurate estimates of thermodynamic derivatives that entail combinations of higher-order moments, as in Eq. (4.3). Despite the deficiencies, a trend towards a slightly negative asymptotic limit seems clearly visible. Overall we thus conclude

$$R_\mu^{\mathrm{HCSW}} = -0.08 \pm 0.12. \quad (4.6)$$

The substantial uncertainty, which does not exclude the possibility $R_\mu = 0$ (although we are inclined to believe a small negative value), is an indication of the confidence level achieved. To obtain better estimates and to fully reveal the onset of the Yang-Yang anomaly, one will need to investigate much larger system sizes L than those accessed here and longer runs will also be necessary to reduce the statistical uncertainties. The invention of more efficient sampling algo-

rithms, such as those developed for magnetic systems [55], is badly needed for asymmetric fluids. That task, however, remains elusive.

V. CONCLUSIONS

In the simulation studies reported here we have addressed the issue of how best to estimate the critical parameters and, in particular, how to elucidate the universality class of gas-liquid criticality in continuum models of *asymmetric* fluids with no known or existing true (or hidden) axes of symmetry. Specifically, we have considered the hard-core square-well model with moderate-range interactions ($\lambda = b/\sigma = 1.5$): this model is only ''weakly asymmetric,'' comparing reasonably well with real fluids like argon and CO_2: but an important aim of our work has been to devise and test unbiased approaches for application to the fundamental ''restricted primitive model'' (RPM) electrolyte which, indeed, is *strongly asymmetric* (largely by virtue of the low value of its critical density: such studies of the RPM are currently underway [18]).

The first computational problem that arises is to estimate convincingly the location of the critical point including, most crucially, the critical density ρ_c. (Typically, the determination of ρ_c presents a significant difficulty even when interpreting precise data on real fluids: see, e.g., [6].) To this end, we have developed methods of selecting various loci, primarily lying in the *single*-phase region *above* T_c, which as the system size L becomes infinite, must asymptotically approach the true, limiting critical point. Those loci which, by their behavior in the (ρ, T) plane, most directly (and most rapidly as L is increased) approach the critical point, may be treated as ''effective symmetry axes,'' analogous to the axes known exactly in simple (Ising-model) lattice gases [19]. Using these loci, one may apply the unbiased techniques devised for lattice models in [19] to estimate, in the first place, the basic critical exponent ν. This exponent provides both an initial indication of critical universality class and a firm basis for subsequent employment of finite-size scaling techniques. We believe this approach should be applicable in other cases where precise and accurate simulation results are desired.

Given an estimate for ν and well-behaved, asymptotically critical loci, determination of T_c by studying a *range* of different estimators [19] yields a precise value. That, in turn, enables one to make refined estimates of ρ_c of high precision and, we believe, reliability. Significantly, previous finite-size scaling methods of some sophistication (which, however, presuppose Ising-type criticality [25, 26]) are found to provide inaccurate estimates of ρ_c.

It would, indeed, be useful for ''practical'' applications to have some more reliable approaches to the estimation of T_c and ρ_c that call for less computational effort than we have invested. Future work may uncover such methods; but it would seem that the underlying scaling theory would have to recognize that when there is no evident ''gas-liquid symmetry'' present in the system, the asymptotic linear scaling fields are more complex than lattice-gas-based models reveal [1, 6]. Specifically, the *pressure*, as well as the chemical potential and the temperature, must mix into the linear scaling fields [1].

This feature arises because of the presence, in general, of a Yang-Yang anomaly in real fluids and nonsymmetric models [1, 2, 6]: explicitly, if $\mu_\sigma(T)$ is the chemical potential on the phase boundary below T_c, then $(d^2\mu_\sigma/dT^2)$ diverges (like the specific heat C_V) when $T \to T_c^-$. We have endeavored to estimate the relative strength R_μ of such a Yang-Yang anomaly in the hard-core square-well fluid (with $\lambda = 1.5$). Analysis of our data suggests a small negative value $R_\mu \simeq -0.08$ (comparable to CO_2 [1]) but with significant uncertainties. To do better for this model will require the study of larger sizes and longer simulations: that will probably be feasible only with improved algorithms (like those available for lattice models [55]). Nevertheless, the study of other models, such as the RPM, etc., may prove more definitive in this respect.

In summary, although we believe we have made progress, elucidating in a precise way the critical behavior of intrinsically asymmetric systems still presents significant challenges—not only computationally, but experimentally and theoretically also—and might provide yet further surprises.

ACKNOWLEDGMENTS

The interest of Professor Mikhail A. Anisimov and Professor Jan V. Sengers has been appreciated. The support of the National Science Foundation (through Grant No. CHE 99-81772 to M.E.F) and of the Department of Energy, Office of Basic Energy Sciences (through Grant No. DE-FG02-98ER14858 to A.Z.P.) is gratefully acknowledged.

[1] M. E. Fisher and G. Orkoulas, Phys. Rev. Lett. **85**, 696 (2000).
[2] C. N. Yang and C. P. Yang, Phys. Rev. Lett. **13**, 303 (1964).
[3] B. Widom and J. S. Rowlinson, J. Chem. Phys. **52**, 1670 (1970).
[4] See, e.g., N. D. Mermin, Phys. Rev. Lett. **26**, 169 (1971).
[5] J. J. Rehr and N. D. Mermin, Phys. Rev. A **8**, 472 (1973).
[6] G. Orkoulas, M. E. Fisher, and C. Üstün, J. Chem. Phys. **113**, 7530 (2000).
[7] See, e.g., G. Orkoulas and A. Z. Panagiotopoulos, J. Chem. Phys. **110**, 1581 (1999) and references therein.
[8] M. E. Fisher, J. Stat. Phys. **75**, 1 (1994); J. Phys.: Condens. Matter **8**, 9103 (1996).
[9] M. E. Fisher and Y. Levin, Phys. Rev. Lett. **71**, 3826 (1993).
[10] B. P. Lee and M. E. Fisher, Phys. Rev. Lett. **76**, 2906 (1996); M. E. Fisher and B. P. Lee, *ibid.* **77**, 3561 (1996).
[11] G. Stell, J. Stat. Phys. **78**, 197 (1995); J. Phys.: Condens. Matter **8**, 9329 (1996).
[12] G. Stell, in *New Approaches to Problems in Liquid State Theory*, NATO Science Series C Vol. 529, edited by C. Caccamo, J.-P. Hansen, and G. Stell (Kluwer Academic, Dor-

drecht, 1999), p. 71.
[13] A. G. Moreira, M. M. Telo da Gama, and M. E. Fisher, J. Chem. Phys. **110**, 10058 (1999) and references therein.
[14] A. Z. Panagiotopoulos, Fluid Phase Equilibria **76**, 97 (1992).
[15] J. M. Caillol, D. Levesque, and J. J. Weis, Phys. Rev. Lett. **77**, 4039 (1996); J. Chem. Phys. **107**, 1565 (1997).
[16] J. P. Valleau and G. Torrie, J. Chem. Phys. **108**, 5169 (1998).
[17] G. Orkoulas and A. Z. Panagiotopoulos, J. Chem. Phys. **101**, 1452 (1994); **110**, 1581 (1999).
[18] E. Luijten, M. E. Fisher, and A. Z. Panagiotopoulos, J. Chem. Phys. **114**, 5468 (2001), and unpublished.
[19] G. Orkoulas, A. Z. Panagiotopoulos, and M. E. Fisher, Phys. Rev. E **61**, 5930 (2000).
[20] R. Guida and J. Zinn-Justin, J. Phys. A **31**, 8103 (1998).
[21] E. Luijten, H. W. J. Blöte, and K. Binder, Phys. Rev. E **54**, 4626 (1996).
[22] E. Luijten, H. W. J. Blöte, and K. Binder, Phys. Rev. Lett. **79**, 561 (1997); Phys. Rev. E **56**, 6540 (1997).
[23] E. Luijten, H. W. J. Blöte, Phys. Rev. B **56**, 8945 (1997); E. Luijten, Phys. Rev. E **59**, 4997 (1999); E. Luijten and K. Binder, Europhys. Lett. **47**, 311 (1999).
[24] A brief, summary account of our work has been presented in G. Orkoulas, M. E. Fisher, and A. Z. Panagiotopoulos, in *Computer Simulation Studies in Condensed Matter Physics XIII*, 13th Annual Workshop on Recent Developments in Computer Simulation Studies in Condensed Matter Physics, Athens, Georgia, 2000, edited by D. P. Landau, S. P. Lewis, and H. B. Schüttler (Springer, Heidelberg, 2000), p. 167.
[25] A. D. Bruce and N. B. Wilding, Phys. Rev. Lett. **68**, 193 (1992); N. B. Wilding and A. D. Bruce, J. Phys.: Condens. Matter **4**, 3087 (1992).
[26] N. B. Wilding, J. Phys.: Condens. Matter **9**, 585 (1997).
[27] A rather natural locus of effective symmetry, much used in experimental work, is based on linear extrapolation vs T of the coexistence diameter $\overline{\rho}(T)$, defined in Eq. (1.2), up to and beyond T_c. Apart from the uncertain nature of the critical singularities in $\overline{\rho}(T)$ [as discussed after Eq. (1.2)], the diameter, like the coexistence curve itself, is essentially undefined in the near-critical region of a finite-size simulation owing to the necessarily strong rounding and spread of the density distribution. In the RPM, furthermore, the diameter has a very large slope and, it seems likely, significant curvature so that even naive extrapolation is problematical.
[28] P. Labastie and R. L. Whetten, Phys. Rev. Lett. **65**, 1567 (1990); R. E. Kunz and R. S. Berry, Phys. Rev. E **49**, 1895 (1994); R. S. Berry, Nature (London) **393**, 212 (1998).
[29] J. B. Elliott *et al.*, Phys. Lett. B **381**, 35 (1996); J. B. Elliott and A. S. Hirsch, Phys. Rev. C **61**, 054605 (2000); J. B. Elliott *et al.*, Phys. Rev. Lett. **85**, 1194 (2000).
[30] P. Borrmann, O. Mülken, and J. Harting, Phys. Rev. Lett. **84**, 3511 (2000).
[31] A. M. Ferrenberg and R. H. Swendsen, Phys. Rev. Lett. **61**, 2635 (1988); **63**, 1195 (1989).
[32] K. Binder, Z. Phys. B: Condens. Matter **43**, 119 (1981).
[33] C. Borgs and R. Kotecky, J. Stat. Phys. **61**, 79 (1990); Phys. Rev. Lett. **68**, 1734 (1992).
[34] For a discussion of the isothermal-isobaric ensemble see, e.g., W. W. Wood, J. Chem. Phys. **48**, 415 (1968). These points can also be found in T. L. Hill, *Thermodynamics of Small Systems, Parts I and II* (Dover, New York, 1962).
[35] B. A. Berg and T. Neuhaus, Phys. Rev. Lett. **68**, 9 (1992); B. A. Berg and T. Celik, *ibid.* **69**, 2292 (1992).
[36] M. E. Fisher, in *Critical Phenomena*, edited by M. S. Green (Academic, New York, 1971), p. 1, Sec. V.
[37] M. E. Fisher and M. N. Barber, Phys. Rev. Lett. **28**, 1516 (1972).
[38] K. Binder, Ferroelectrics **73**, 43 (1987); Rep. Prog. Phys. **50**, 783 (1987).
[39] *Finite Size Scaling and Numerical Simulations of Statistical Systems*, edited by V. Privman (World Scientific, Singapore, 1990).
[40] A. M. Ferrenberg and D. P. Landau, Phys. Rev. B **44**, 5081 (1991).
[41] *The Monte Carlo Method in Condensed Matter Physics*, edited by K. Binder (Springer-Verlag, Berlin, 1992).
[42] K. Chen, A. M. Ferrenberg, and D. P. Landau, J. Appl. Phys. **73**, 5488 (1993); Phys. Rev. B **48**, 3249 (1993).
[43] K. Binder, Rep. Prog. Phys. **60**, 487 (1997).
[44] B. Widom, J. Chem. Phys. **43**, 3898 (1965).
[45] M. Vicentini-Missoni, J. M. H. Levelt Sengers, and M. S. Green, J. Res. Natl. Bur. Stand., Sect. A **73**, 563 (1969).
[46] See [19] and references therein.
[47] L. Vega, E. de Miguel, L. F. Rull, G. Jackson, and I. A. McLure, J. Chem. Phys. **96**, 2296 (1992).
[48] N. V. Brilliantov and J. P. Valleau, J. Chem. Phys. **108**, 1115 (1998); **108**, 1123 (1998).
[49] H. E. Stanley, in *Phase Transitions and Critical Phenomena*, edited by C. Domb and M. S. Green (Academic, London, 1974), Vol. 3, Chap. 7.
[50] M. E. Fisher and S.-Y. Zinn, J. Phys. A **31**, L629 (1998).
[51] J. M. H. Levelt Sengers and S. C. Greer, Int. J. Heat Mass Transf. **15**, 1865 (1972).
[52] I. M. Abdulagatov, L. N. Levina, Z. R. Zakaryaev, and O. N. Mamchenkova, Fluid Phase Equilibria **127**, 205 (1997).
[53] E. M. Gaddy, Ph.D. thesis, The American University, Washington, D.C., 1978; E. M. Gaddy and J. A. White, Phys. Rev. A **26**, 2218 (1982).
[54] We also examined the simulation data for $\check{C}_p(T,\rho;L)$ and $\check{C}_\mu(T,\rho;L)$ for various values of $\rho \neq \rho_c$. The observed behavior is fairly complex; but it can be understood as arising from the finite-size rounding of singularities and discontinuities and from the linear dependence on density implied by Eq. (4.2) in the thermodynamic limit, when it reads, in an obvious notation, $\check{C}_V(T,\rho)=\check{p}''_\sigma(T)-\rho\check{\mu}''_\sigma(T)$. In a sufficiently large and precise simulation, further significant information regarding the Y-Y anomaly may well be extractable from studying these functions. At the level achieved, however, further investigation did not seem promising.
[55] R. H. Swendsen and J.-S. Wang, Phys. Rev. Lett. **58**, 86 (1987); U. Wolff, *ibid.* **60**, 1461 (1988); **62**, 361 (1989).